ChemComm

Chemical Communications

www.rsc.org/chemcomm

Volume 48 | Number 31 | 18 April 2012 | Pages 3673–3788

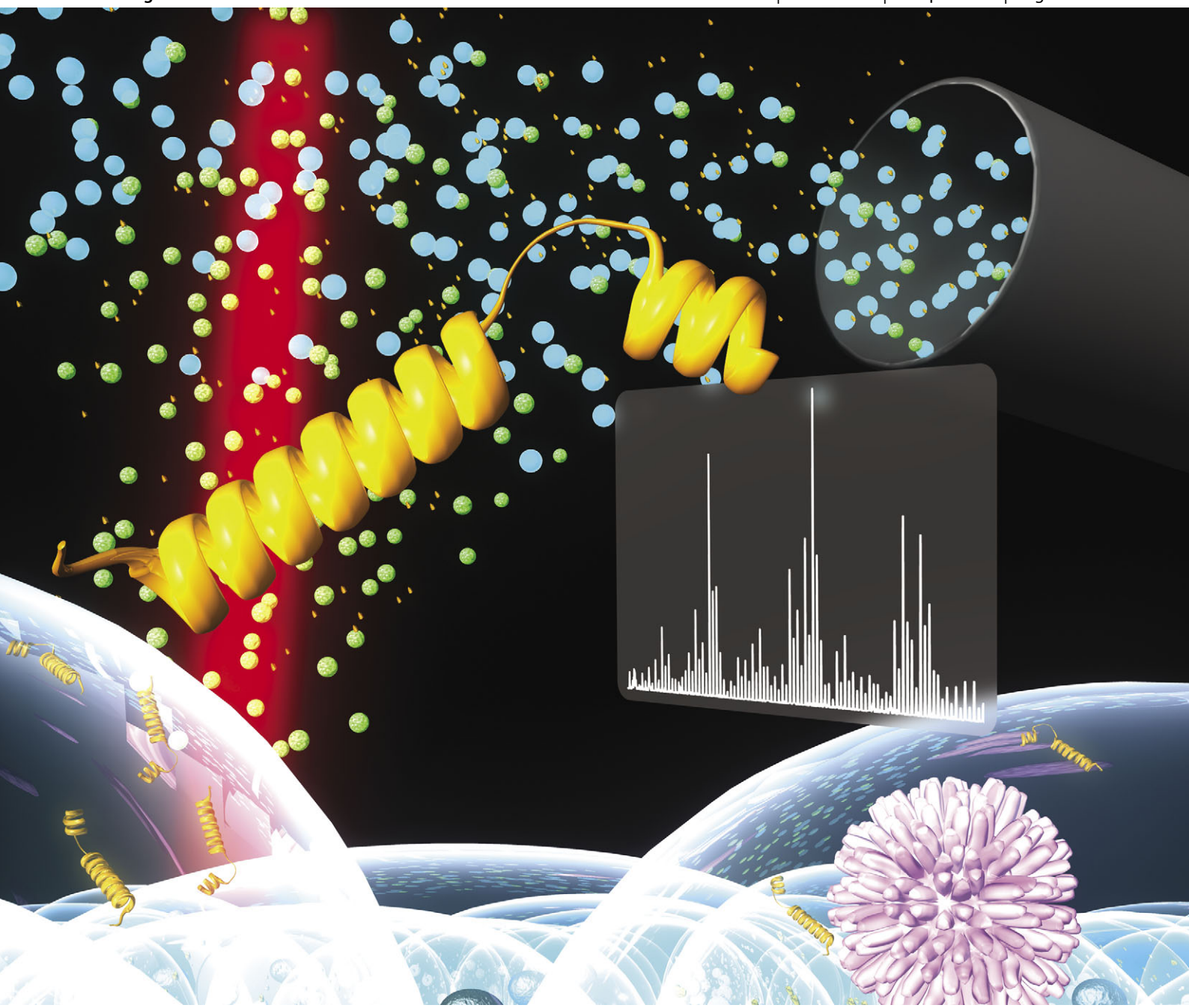

ISSN 1359-7345

RSC Publishing

COMMUNICATION

Vertes *et al.*

Rapid, non-targeted discovery of biochemical transformation and biomarker candidates in oncovirus-infected cell lines using LAESI mass spectrometry

1359-7345(2012)48:31;1-A

ChemComm

Dynamic Article Links

Cite this: *Chem. Commun.*, 2012, **48**, 3700–3702

www.rsc.org/chemcomm

COMMUNICATION

Rapid, non-targeted discovery of biochemical transformation and biomarker candidates in oncovirus-infected cell lines using LAESI mass spectrometry†

Bindesh Shrestha,[a] Prabhakar Sripadi,[a] Callee M. Walsh,[b] Trust T. Razunguzwa,[b] Matthew J. Powell,[b] Kylene Kehn-Hall,[c] Fatah Kashanchi[c] and Akos Vertes*[a]

Received 21st November 2011, Accepted 1st December 2011
DOI: 10.1039/c2cc17225a

Finding insights into how viruses hijack metabolic processes and biomarkers for viral diseases often require hypotheses about target compounds and/or labelling techniques. Here we present a method based on laser ablation electrospray ionization mass spectrometry to rapidly identify potential protein and metabolite biomarkers of oncovirus infection in B lymphocytes.

Ambient ionization mass spectrometry (MS) methods, such as desorption electrospray ionization,[1,2] direct analysis in real time,[3] and laser ablation electrospray ionization (LAESI),[4–6] provide a means to rapidly profile the metabolic state of live cells with minimal sample preparation. Identifying transformations induced by the presence of a viral infection, however, requires a method that provides a snapshot of changes in the abundances of diverse biochemical components, including proteins, lipids and small metabolites. Direct analysis of brain tissue sections by LAESI-MS has been shown to simultaneously detect these classes of compounds.[7] Identifying biomarker candidates from the resulting complex mass spectra, however, is time consuming and tedious. Multivariate statistical methods, such as orthogonal projections to latent structures discriminant analysis (OPLS-DA) can be used to identify the ions responsible for most of the variance between the mass spectra of control and diseased cells. The workflow of this biomarker discovery method, which combines LAESI-MS and OPLS-DA, starts with acquisition of ambient MS data by LAESI-MS, followed by batch processing of the acquired mass spectra. Potential biomarkers are discerned by processing the relative intensity values with multivariate statistical methods (*e.g.*, OPLS-DA). The biomarker candidates are putatively identified *via* searching metabolomics and lipidomics databases (*e.g.*, Human Metabolome Database (HMDB), or in-house databases). Identifications are confirmed by tandem MS analysis.

[a] *Department of Chemistry, W. M. Keck Institute of Proteomics Technology and Applications, The George Washington University, Washington D.C, USA. E-mail: vertes@gwu.edu; Fax: +1-202-994-5873; Tel: +1-202-994-2717*
[b] *Protea Biosciences, 955 Hartman Run Road, Morgantown, WV 26505*
[c] *Department of Molecular and Microbiology, National Center for Biodefense and Infectious Diseases, George Mason University, Manassas, VA 20110, USA*
† Electronic supplementary information (ESI) available. See DOI: 10.1039/c2cc17225a

Metabolites are known to be altered in cancerous cells and tissues, resulting in depletion of nutrients, accumulation of immunosuppressive metabolites, modulation of proliferation and apoptosis, and oxidative stress.[8–11] Specifically, multiple studies have demonstrated that phospholipid levels are altered in normal *versus* tumour tissues, affecting the dynamics of the cell membrane.[12,13] Phospholipids are structural components of the plasma membrane as well as critical signalling molecules. Variations in phospholipid levels can influence membrane fluidity and permeability, which affects transport systems and the activity of membrane-bound enzymes.[14,15] Therefore, the analysis of these metabolites in oncovirus-infected cells is of particular interest.

Here we report the use of LAESI-MS combined with multivariate statistical tools to identify biomarker candidates from oncovirus-infected cells. We are specifically interested in understanding the metabolic differences between B-lymphocytes that are latently infected with Kaposi's sarcoma-associated herpesvirus (KSHV), which are known as BCBL-1 cells, and non-KSHV infected B-lymphocytes (BJAB cells). KSHV infection causes at least three distinct diseases, Kaposi's sarcoma, primary effusion lymphoma (PEL), and multicentric Castleman's disease (MCD). Kaposi's sarcoma is a cancer which has been commonly known in the past as an AIDS defining illness for HIV infected patients and presents with characteristic purple/brown lesions. PEL and MCD are diseases caused by the excessive production of B lymphocytes.[16,17]

Both BCBL-1 and BJAB cells were grown in suspension at 37 °C under 5% CO_2 in RPMI 1640 medium containing 10% fetal bovine serum, L-glutamine (2 mM), penicillin (100 units/mL) and streptomycin (100 mg mL^{-1}) to contain approximately the same number of cells. Prior to LAESI-MS analysis, the cells were washed twice with PBS and pelleted by centrifugation at 2000 rpm to obtain $\sim 10^6$ cells per pellet. From these pellets, 10 μL samples were loaded onto clean microscope slides for the LAESI-MS experiments. The LAESI-MS system used was similar to ones that have been described in detail elsewhere.[18,19] Briefly, laser ablation at 2.94 μm was performed with an optical parametric oscillator with average energy output of 0.3 mJ/pulse at the target. Electrospray was produced by applying 2800 V to 50% methanol solution containing 0.1% (v/v) acetic acid. The samples were typically measured in five biological replicates (different aliquots from the same passage

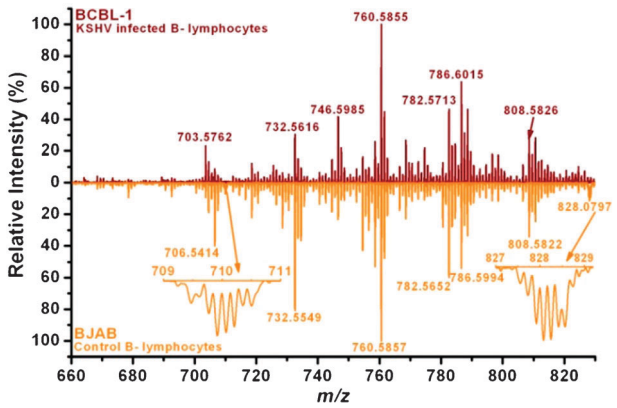

Fig. 1 LAESI mass spectra (positive ion mode) pertaining to the lipid region (m/z 660 to 830) in BCBL-1 cells (top) and BJAB cells (bottom).

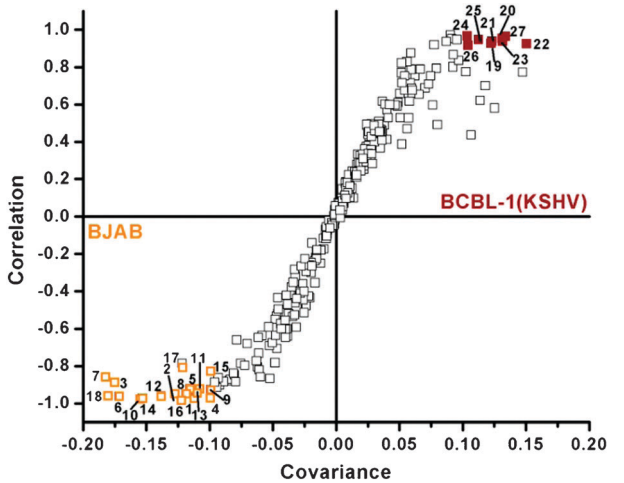

Fig. 2 S-plot of ions found within the lipid region (m/z 660 to 830) for both BJAB and BCBL-1 cells. The highlighted, numbered ions exhibit correlation in excess of ±0.8 and covariance in excess of ±0.1 and are responsible for most of the variance between mass spectra of BCBL-1 and BJAB cells shown in Fig. 1.

of the cell culture). In addition, the experiments were repeated on different generations of the same cell lines grown several months apart. The resulting ions were analyzed by a time-of-flight mass spectrometer in positive mode. LAESI mass spectra were initially processed by MassLynx software. Multivariate statistical analyses were performed on the processed mass spectra with the Extended Statistics module of MarkerLynx software.

LAESI-MS analysis of BCBL-1 and BJAB cells indicated several differences in relative signal intensity. The most notable changes occurred for ions found within the lipid region of the mass spectrum from m/z 660 to 830 (see Fig. 1). Fig. S2 in the electronic supplement compares replicates. In order to simplify the identification of differences between the two cell lines, the OPLS-DA with Pareto scaling was implemented on similarly processed mass spectra.

The supervised OPLS-DA method can be applied to the affected and control groups to simplify the interpretation of separation. OPLS-DA is helpful in the identification of potential biomarkers because it can separate both intra-class variations and inter-class variations in the datasets.[20] In addition, it is well-suited for metabolomics studies which generally have a large dynamic range but in which the majority of affected compounds are present at low concentration. In the OPLS-DA S-plot, covariance, an indicator of an ion's contribution to the observed differences, and correlation, an indicator of reliability, are plotted to distinguish statistically significant ions, which could be potential biomarker candidates.[20] Ions that exhibit a high correlation and a high covariance are statistically significant with a small confidence interval. These ions are located within the wings of the S-plot and contribute most to the differences between samples.

OPLS-DA analysis of the ions within the lipid region is summarized in the S-plot in Fig. 2. Ions that contribute most to the spectral differences between BJAB and BCBL-1 cells are indicated with shading and numerals. The compounds were identified using database searches and ion fragmentation experiments and are shown in Fig. 3 and Table S1. Many phospholipids were identified as contributing to signal differences between the cell types, and, specifically, several phosphatidylcholines were downregulated in virally-infected cells. This observation is in agreement with a recent study which demonstrated that phosphatidylcholine species in T lymphocytes are reduced after infection with human T-lymphotropic virus type 1.[4] The alterations in phosphatidylcholine species may provide changes to cell membrane permeability that are advantageous for viral infection. In addition, changes in the fatty acid composition of phosphatidylcholines are commonly observed in cancer cells.[12,13,21]

A multiply-charged small protein exhibited the largest difference in expression between the two cell types. Ions of m/z 710, 828, 993 and 1241 having +7, +6, +5, +4 charge states, respectively, correspond to a low molecular weight protein with a nominal monoisotopic mass of 4960 Da, which was assigned to thymosin β4 (Tβ4). Expression of Tβ4 was reduced by greater than 90% in BCBL-1 cells with respect to

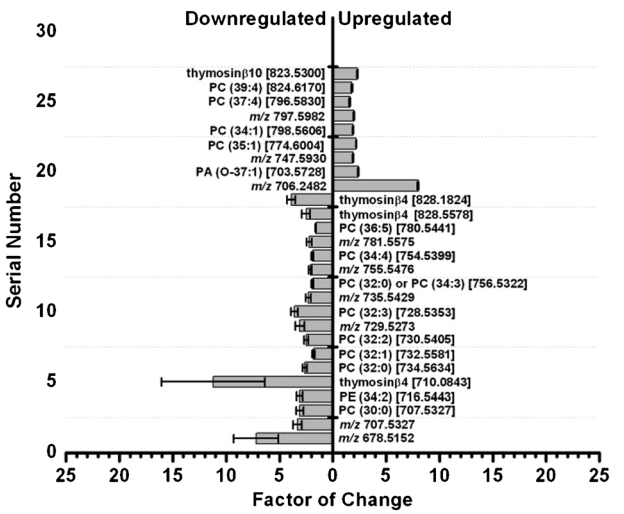

Fig. 3 Identification of ions detected in the wings of the S-plot. The grey bars represent the relative up- and downregulation of compounds in BCBL-1 cells with respect to BJAB cells. Indicated on each bar is the standard error of the mean, the name of the identified compound, and its m/z value. The serial number corresponds to labelled points in the S-plot (Fig. 2).

BJAB cells specifically for the +7 charge state. In addition to BJAB and BCBL-1 cells, differences in the expression of Tβ4 were observed for HML-1, HUT, HeLa, Jurkat and C81 cell lines (see Fig. S1). In recent years, it has been shown that Tβ4 facilitates actin filament growth,[22] promotes wound healing and decreases inflammation.[23] The results obtained by LAESI-MS for the Tβ4 peptide were independently tested by protein immunoblotting. The SDS-PAGE and western blot analysis with anti-Tβ4 antibody were performed on whole-cell protein lystates (25 or 50 μg) of H9, BJAB, and BCBL-1 cells (see Fig. S3A). The SDS band for positive control of Tβ4 peptide included in the first lane is the most pronounced as expected. In cell lysates, the bands for the BJAB cells clearly indicate higher intensities, hence a higher concentration, than those of the KSHV infected BCBL-1 cells. Another protein species, actin, was observed with the same intensities for all the cell lines confirming that the observed changes in Tβ4 were not due to a concentration gradient in the cell lysates. Fig. S3B shows the results of the total PC assay for whole cell lysates in BJAB and BCBL-1 cells. Weaker fluorescence for the total PC in BCBL-1 cells by almost a factor of two indicates an overall downregulation of these species in the infected case. Summing the LAESI-MS peak areas of the 12 PC species identified in Fig. 3 for the two cell lines shows a reduction from 4003 ± 545 to 2040 ± 580 in case of BJAB and BCBL-1, respectively. The ratio of these values is in close to quantitative agreement with the change seen in Fig. S3B. It is worth pointing out that the LAESI-MS results contain significantly more information than the total PC assay, as they indicate slight upregulation for four PCs and downregulation for eight PCs with a net result of downregulation for the total PC content.

Furthermore, Tβ4 suppresses NFκB phosphorylation, activity, and nuclear translocation in cultured human corneal epithelial cells stimulated with TNF-α.[24] Tβ4 acts on many cell types and has many different biological effects beyond growth and migration, including being anti-apoptotic, antimicrobial, and antifibrotic. Our results show that Tβ4 is significantly downregulated in KSHV-infected cells. We believe that this may be the virus' innate defense mechanism to upregulate the NFkB pathway (such as cytokines) that is observed with the infection of the host. The downregulation of Tβ4 causes increased NFkB, which is necessary for the anti-apoptotic pathway and could contribute to overall survival of these cancer cells. It is unclear at this point which NFkB genes are regulated by Tβ4 that could contribute to the survivability of these cells. Future experiments should be able to distinguish between these two distinct roles and how Tβ4 modulates cell replication in KSHV infected cells.

LAESI-MS combined with multivariate statistical analysis is a quick and effective method to provide insight into biochemical transformations and for non-targeted biomarker discovery in viral infection. This method is demonstrated here using cell lines exhibiting differences in the levels of phospholipids and small proteins. After biomarkers are validated with functional studies, LAESI-MS could serve as a rapid screening platform for early diagnosis of disease.

The authors acknowledge financial support from the Office of Basic Energy Sciences, U.S. Department of Energy (DE-FG02-01ER15129), Protea Biosciences, Inc., and the George Washington University Selective Excellence Fund. One of the authors (P. S.) thanks the Director of the Indian Institute of Chemical Technology, Hyderabad, and the Council of Scientific and Industrial Research, India, for granting leave.

Notes and references

1 Z. Takáts, J. M. Wiseman and R. G. Cooks, *J. Mass Spectrom.*, 2005, **40**, 1261–1275.
2 Y. Song, N. Talaty, W. A. Tao, Z. Pan and R. G. Cooks, *Chem. Commun.*, 2007, 61–63.
3 C. Y. Pierce, J. R. Barr, R. B. Cody, R. F. Massung, A. R. Woolfitt, H. Moura, H. A. Thompson and F. M. Fernandez, *Chem. Commun.*, 2007, 807–809.
4 P. Sripadi, B. Shrestha, R. L. Easley, L. Carpio, K. Kehn-Hall, S. Chevalier, R. Mahieux, F. Kashanchi and A. Vertes, *PLoS One*, 2010, **5**, e12590.
5 B. Shrestha and A. Vertes, *Anal. Chem.*, 2009, **81**, 8265–8271.
6 B. Shrestha, J. M. Patt and A. Vertes, *Anal. Chem.*, 2011, **83**, 2947–2955.
7 P. Nemes, A. S. Woods and A. Vertes, *Anal. Chem.*, 2010, **82**, 982–988.
8 K. Singer, E. Gottfried, M. Kreutz and A. Mackensen, *Cancer Immunol. Immunother.*, 2011, **60**, 425–431.
9 S. Ganti, S. L. Taylor, K. Kim, C. L. Hoppel, L. Guo, J. Yang, C. Evans and R. H. Weiss, *Int. J. Cancer*, 2011.
10 M. P. Lisanti, U. E. Martinez-Outschoorn, B. Chiavarina, S. Pavlides, D. Whitaker-Menezes, A. Tsirigos, A. Witkiewicz, Z. Lin, R. Balliet, A. Howell and F. Sotgia, *Cancer Biol. Ther.*, 2010, **10**, 537–542.
11 M. M. Wright, A. G. Howe and V. Zaremberg, *Biochem. Cell Biol.*, 2004, **82**, 18–26.
12 A. Preetha, R. Banerjee and N. Huilgol, *Journal of Cancer Research and Therapeutics*, 2005, **1**, 180–186.
13 A. Preetha, N. Huilgol and R. Banerjee, *Biomed. Pharmacother.*, 2005, **59**, 491–497.
14 A. A. Spector and M. A. Yorek, *J. Lipid Res.*, 1985, **26**, 1015–1035.
15 J. Tepsic, V. Vucic, A. Arsic, V. Blazencic-Mladenovic, S. Mazic and M. Glibetic, *Eur. J. Appl. Physiol.*, 2009, **107**, 359–365.
16 M. Arguello, S. Paz, E. Hernandez, C. Corriveau-Bourque, L. M. Fawaz, J. Hiscott and R. Lin, *The Journal of Immunology*, 2006, **176**, 7051–7061.
17 E. Cesarman, Y. Chang, P. S. Moore, J. W. Said and D. M. Knowles, *N. Engl. J. Med.*, 1995, **332**, 1186–1191.
18 P. Nemes and A. Vertes, *Anal. Chem.*, 2007, **79**, 8098–8106.
19 B. Shrestha, P. Nemes, J. Nazarian, Y. Hathout, E. P. Hoffman and A. Vertes, *Analyst*, 2010, **135**, 751–758.
20 S. Wiklund, E. Johansson, L. Sjostrom, E. J. Mellerowicz, U. Edlund, J. P. Shockcor, J. Gottfries, T. Moritz and J. Trygg, *Anal. Chem.*, 2008, **80**, 115–122.
21 M. Hilvo, C. Denkert, L. Lehtinen, B. Mueller, S. Brockmoeller, T. Seppaenen-Laakso, J. Budczies, E. Bucher, L. Yetukuri, S. Castillo, E. Berg, H. Nygren, M. Sysi-Aho, J. L. Griffin, O. Fiehn, S. Loibl, C. Richter-Ehrenstein, C. Radke, T. Hyoetylaeinen, O. Kallioniemi, K. Iljin and M. Oresic, *Cancer Res.*, **71**, 3236–3245.
22 D. Pantaloni and M. F. Carlier, *Cell*, 1993, **75**, 1007–1014.
23 G. Sosne, P. L. Christopherson, R. P. Barrett and R. Fridman, *Invest. Ophthalmol. Visual Sci.*, 2005, **46**, 2388–2395.
24 G. Sosne, P. Qiu, P. L. Christopherson and M. K. Wheater, *Exp. Eye Res.*, 2007, **84**, 663–669.

ChemComm

Electronic Supplementary Information COMMUNICATION

Rapid, non-targeted discovery of biochemical transformation and biomarker candidates in oncovirus-infected cell lines using LAESI mass spectrometry

Bindesh Shrestha[a], Prabhakar Sripadi[a], Callee M. Walsh[b], Trust T. Razunguzwa[b], Matthew J. Powell,[b] Kylene Kehn-Hall,[c] Fatah Kashanchi[c] and Akos Vertes*[a]

[a]Department of Chemistry, W.M. Keck Institute of Proteomics Technology and Applications, The George Washington University, Washington D.C, USA. Fax: +1-202-994-5873 Tel: +1-202-994-2717; E-mail: vertes@gwu.edu

[b]Protea Biosciences, 955 Hartman Run Road, Morgantown, WV 26505

[c]Department of Molecular and Microbiology, National Center for Biodefense and Infectious Diseases, George Mason University, Manassas, VA 20110, USA.

Table S1. Putative assignments of ions corresponding to the numbered points found in the wings of the S-plotin Figure 2 and the histogram in Figure 3. Table S1 only shows the assignments selected on the basis of exhibiting the most variance in the mass spectra between the affected and control cell lines. Numerous other ions were also detected but did not show major changes between the two groups.

SN	Putative Assignments	Ion	Monoisotopic *m/z*	Measured Average *m/z*	Δm (mDa)	Factor of Change	
						Down regulated	Up regulated
1	unassigned			678.5152		7.2±2.1	
2	unassigned			707.5327		3.3±0.4	
3	PC(30:0)	$C_{38}H_{76}NO_8P+H^+$	706.5387	706.5423	3.6	3.1±0.3	
4	PE(34:2)	$C_{39}H_{74}NO_8P+H^+$	716.5230	716.5443	21.3	3.1±0.3	
5	thymosin β4	$C_{212}H_{350}N_{56}O_{78}S_1+7H^{+7}$	710.0806	710.0843	3.7	11.2±4.8	
6	PC(32:0)	$C_{40}H_{80}NO_8P+H^+$	734.5700	734.5634	-6.6	2.6±0.2	
7	PC(32:1)	$C_{40}H_{78}NO_8P+H^+$	732.5543	732.5581	3.8	1.8±0.1	
8	PC(32:2)	$C_{40}H_{76}NO_8P+H^+$	730.5387	730.5405	1.8	2.5±0.2	
9	unassigned			729.5273		3.1±0.4	
10	PC(32:3)	$C_{40}H_{74}NO_8P+H^+$	728.5230	728.5353	12.3	3.6±0.3	
11	unassigned			735.5429		2.3±0.2	
12	PC(34:3) PC(32:0)	$C_{42}H_{78}NO_8P+H^+$ $C_{40}H_{80}NO_8P+Na^+$	756.5543 756.5519	756.5322	-22.1 -19.7	1.9±0.1	
13	unassigned			755.5476		2.1±0.2	
14	PC(34:4)	$C_{42}H_{76}NO_8P+H^+$	754.5387	754.5399	1.2	1.9±0.1	
15	unassigned			781.5575		2.2±0.3	
16	PC(36:5)	$C_{44}H_{78}NO_8P+H^+$	780.5543	780.5441	-10.2	1.6±0.1	
17	thymosin β4	$C_{212}H_{350}N_{56}O_{78}S_1+6H^{+6}$	828.5954	828.5778	-17.6	2.5±0.4	
18	thymosin β4	$C_{212}H_{350}N_{56}O_{78}S_1+6H^{+6}$	828.2594	828.1824	-77.0	3.9±0.4	
19	unassigned			706.2482			8.0±0.1
20	PA (O-37:1)	$C_{40}H_{79}O_7P+H^+$	703.5641	703.5728	8.7		2.4±0.0
21	unassigned			747.5930			1.9±0.0
22	PC(35:1)	$C_{43}H_{84}NO_8P+H^+$	774.6012	774.6004	-0.8		2.2±0.0
23	PC(34:1)	$C_{42}H_{82}NO_8P+K^+$	798.5414	798.5606	19.2		1.9±0.0
24	unassigned			797.5982			2.0±0.0
25	PC(37:4)	$C_{45}H_{82}NO_8P+H^+$	796.5856	796.5830	-2.6		1.6±0.0
26	PC(39:4)	$C_{47}H_{86}NO_8P+H^+$	824.6170	824.5488	-68.2		1.8±0.1
27	thymosin β10	$C_{211}H_{353}N_{57}O_{76}S+6H^{+6}$	823.5976	823.5300	-67.6		2.3±0.0

[a] The monoisotopic masses were calculated using the NIST Isotope Calculator package (ISOFORM, Version 1.02) or MolE - Molecular Mass Calculator v2.02 (http://library.med.utah.edu/masspec/mole.htm). The measured *m/z* values were obtained by averaging *m/z* values in mass spectra from parallel samples.

[b] Glycerophosphocholines (PC), glycerophosphates (PA), and phosphatidylethanolamines (PE) species are identified by the total length of the acyl chain(s) and the number of double bonds in parentheses.

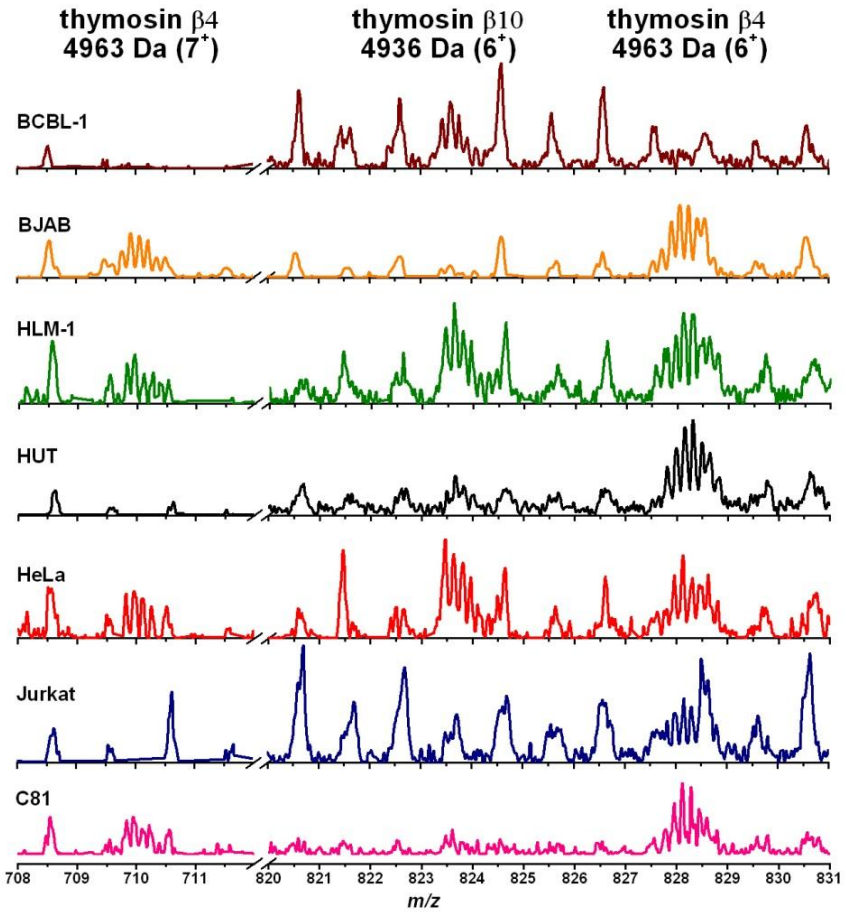

Fig. S1 LAESI-MS analysis of seven different cell lines indicates differences in expression of thymosin β4 and β10. Multiply-charged ion peaks with +6 charge state at ~ *m/z* 823 were assigned to thymosin β10. Ions with charge states of +7 and +6 at ~ *m/z* 710 and 828, respectively, were assigned to thymosin β4. Thymosin β4 expression is reduced in BCBL-1 cells, while thymosin β10 expression is reduced in BJAB cells.

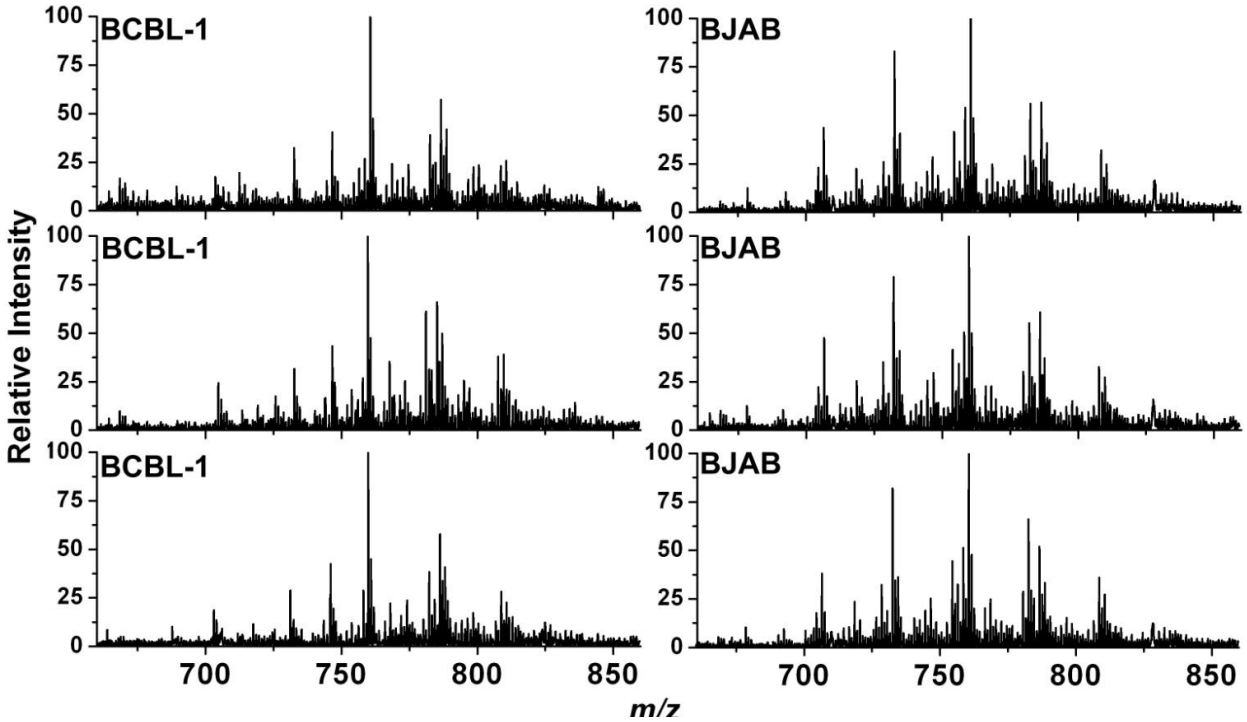

Fig. S2 Comparison of technical variance (spectra within columns) and biological variance (spectra between columns) for LAESI-MS analysis of BCBL-1 and BJAB cell pellets. Differences between the two cell-lines clearly exceed the variations for a given cell line.

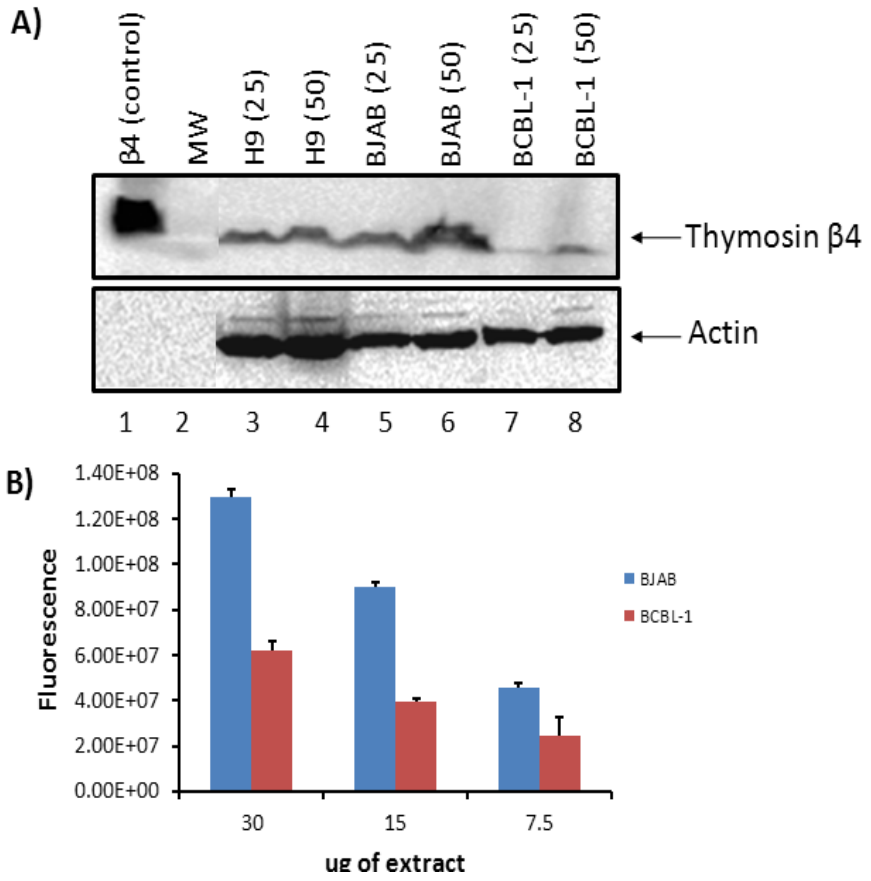

Fig. S3 A) Anti-Tβ4 western blot of lysates from H9 T-cells, BJAB, and BCBL-1 point to lower concentrations of Tβ4 in the infected B cells. B) Lysates from BJAB and BCBL-1 cells assayed for total PC indicate downregulation in the infected cells.